

# High Temperature Ferromagnetic-Ferroelectric Multiferroicity in Strained BiMnO<sub>3</sub>

X. Z. Lu, X. G. Gong, and H. J. Xiang\*

Key Laboratory of Computational Physical Sciences (Ministry of Education), State

Key Laboratory of Surface Physics, and Department of Physics, Fudan University,

Shanghai 200433, P. R. China

## ABSTRACT

Multiferroics with the coexistence of ferroelectric and ferromagnetic orders are ideal candidates for magnetoelectric applications. Unfortunately, only very few ferroelectric-ferromagnetic multiferroics (with low magnetic critical temperature) were discovered. Here we perform first principles calculations to investigate the effects of the epitaxial strain on the properties of BiMnO<sub>3</sub> films grown along the pseudocubic [001] direction. Unlike the ground state with the centrosymmetric  $C2/c$  space group in bulk, we reveal that the tensile epitaxial strain stabilizes the ferromagnetic and ferroelectric  $Cc$  state with a large polarization ( $P > 80 \mu\text{C}/\text{cm}^2$ ) and high Curie temperature (estimated  $T_c \sim 395 \text{ K}$ ). More importantly, there is a novel intrinsic magnetoelectric coupling in the multiferroic  $Cc$  state with the easy magnetization axis controllable by the external electric field.

## INTRODUCTION

In recent years, multiferroics, displaying magnetic, polar, and elastic order parameters simultaneously, have attracted numerous research interests<sup>1</sup>. Although magnetoelectric multiferroics initially refers to a material which is simultaneously ferromagnetic (FM) and ferroelectric (FE), there are only very few FM-FE multiferroics:  $\text{EuTiO}_3$  under large biaxial strain could be FE ferromagnet with a FM Curie temperature 4.24 K<sup>2</sup>; It was predicted that  $\text{SrMnO}_3$  could be driven by epitaxial strain to a multiferroic FM-FE state<sup>3</sup> with the estimated magnetic Curie temperature around 92 K within the mean field theory. For realistic applications, it is desirable to discover or design a room-temperature FM-FE multiferroics with a strong coupling between FE and FM orders.

Among various candidates for FM-FE multiferroics, perovskite-type  $\text{BiMnO}_3$  is special because of the initially predicted coexistence of ferromagnetic and ferroelectric order in this system<sup>4</sup>. Although there was no doubt on its ferromagnetism<sup>5-12</sup>, controversies on its ferroelectricity arose from the most recent experimental and theoretical investigations<sup>11-14</sup>, which demonstrated that  $\text{BiMnO}_3$  crystallizes in a centrosymmetric space group  $C2/c$ . Therefore, it is most likely that there is no ferroelectricity in bulk  $\text{BiMnO}_3$ . In this work, we propose to tune the magnetic and polar order in  $\text{BiMnO}_3$  thin films by epitaxial strain, which is motivated by the recent studies on epitaxial perovskite thin films<sup>2,3,15-19</sup> showing that strain could tune the magnetic and polar order. To the best of our knowledge, the properties of the epitaxial pseudocubic [001]-oriented  $\text{BiMnO}_3$  thin film are not fully understood both

experimentally and theoretically.

In this article, we carry out comprehensive first principles studies to investigate the effects of the epitaxial strain on the properties of BiMnO<sub>3</sub> films grown on the cubic substrate along the pseudocubic [001] direction. A series of phase transitions occur in the studied strain region such as a transition between the AFM insulating FE phase and FM metallic phase and a transition between the FM-PE phase and FM-FE phase. Furthermore, there is a novel intrinsic magnetoelectric coupling in the FM-FE *Cc* state with the calculated polarization  $P > 80 \text{ } \mu\text{C}/\text{cm}^2$  and estimated Curie temperature  $T_c \sim 395 \text{ K}$ .

## METHODS

Total energy calculations are based on the density functional theory (DFT) plus the on-site repulsion (U) method<sup>20</sup> within the generalized gradient approximation with the revised Perdew-Becke-Erzenhof (PBEsol) parametrization<sup>21</sup> on the basis of the projector augmented wave method<sup>22</sup> encoded in the Vienna ab initio simulation package<sup>23</sup>. The plane-wave cutoff energy is set to 700 eV and  $4 \times 4 \times 3$  *k*-point mesh is used for the 20-atom  $\sqrt{2} \times \sqrt{2} \times 2$  cell. We discuss the results obtained with the on-site repulsion  $U = 4 \text{ eV}$  (see Part 2 of SI) and the exchange parameter  $J = 1 \text{ eV}$  on Mn. For the calculation of electric polarization, the Berry phase method<sup>24</sup> is used.

The lattice vectors used in this study are  $\mathbf{a} = a_s\mathbf{x} - a_s\mathbf{y}$ ,  $\mathbf{b} = a_s\mathbf{x} + a_s\mathbf{y}$  and  $\mathbf{c} = \delta_1\mathbf{x} + \delta_2\mathbf{y} + (2a_s + \delta_3)\mathbf{z}$ , where  $a_s$  is the pseudocubic lattice constant of the studied system at a given strain, and ( $\mathbf{x}$ ,  $\mathbf{y}$ ,  $\mathbf{z}$ ) are defined within the pseudocubic setting.

Epitaxial strain is then defined as  $(a_s - a_0)/a_0$ , where  $a_0$  (3.938 Å in this study) is assumed to be the pseudocubic lattice constant of bulk structure with  $C2/c$  space group under a volume-conserving transformation. According to the previously reported possible stable perovskite structures under epitaxial strain<sup>3,16-19,25-27</sup>, we have investigated the BiMnO<sub>3</sub> thin films in the  $I4/mcm$ ,  $Imma$ ,  $R\bar{3}c$ ,  $C2/m$ ,  $Pnma$ ,  $Ima2$ ,  $C2$ ,  $Cc$ ,  $Pmc2_1$  space groups with the FM, A-type AFM (A-AFM), G-type AFM (G-AFM), C-type AFM (C-AFM) spin orders. To obtain the initial structures of the different space groups, we use the method described by Stokes *et al.*<sup>28</sup>. In order to obtain the minimum-energy configuration in a given space group, we optimize the length and direction of the out-of-plane lattice vector ( $c$  lattice vector) and the internal ionic positions until Hellman-Feynman forces are less than 0.01 eV/Å. For the property calculations, we focus on the lowest energy phases in the studied strain range. Curie ( $T_C$ ) and Néel ( $T_N$ ) temperatures are estimated using mean field theory, in which the in-plane nearest-neighbor ( $J_1$ ) and out-of-plane nearest-neighbor ( $J_2$ ) spin exchange interactions are considered and extracted from the energy differences between the FM, A-AFM, G-AFM, C-AFM orders (see Part 1 of SI).

## RESULTS AND DISCUSSION

The total energies of the lowest energy phases, as a function of epitaxial strain from  $-7\%$  to  $7\%$ , are shown in Figure 1. For any strain, the G-AFM and C-AFM states are in much higher energy than the FM and A-AFM states. Thus, they are not shown in Figure 1. For comparison, the total energies of the FM  $C2/c$  phase under the

strain ranging from -4% to 3% are also shown in Figure 1. When simulating epitaxial strain on the  $C2/c$  structure with 40 atoms, we use the same method as adopted in ref 29, namely, “volume-conserving” method. The electric polarizations, magnetic Curie/Néel temperatures, band gaps and  $c$ -lattice parameters for these lowest energy phases are shown in Figure 2. Our results, as discussed in the followings, are different from those obtained by Hatt *et al.*<sup>29</sup>, who examined the effects of strain on  $\text{BiMnO}_3$  by applying the biaxial strain to the experimental  $C2/c$  structure and concluded that  $\text{BiMnO}_3$  remains centrosymmetric and non-polar.

As can be seen in Figure 1, if the strain is small, i.e., between -1.5% and 2%, the orthorhombic centrosymmetric  $Pnma$  structure has the lowest energy, for which the FM order is the spin ground state. Although the space group of  $\text{BiMnO}_3$  has been changed from  $C2/c$  to  $Pnma$ , the unusual FM order remains to be the spin ground state in contrast to other perovskite materials where usually the AFM states prevail, e.g.,  $\text{LaMnO}_3$  with the same space group has the A-AFM spin order. The FM order is further confirmed by the calculated spin exchange parameters (see Part 1 of SI). Interestingly, the  $Pnma$  structure was also found in the polycrystalline  $\text{BiMnO}_3$  samples at high temperature<sup>8</sup>. With increasing strain, the FM  $Pnma$  structure becomes unstable, with a first-order phase transition into the FM  $Cc$  phase. Above the transitional point of  $\sim 2\%$ , the longer Mn-O lengths and Mn-O-Mn angles of the octahedral in the FM  $Pnma$  structure change suddenly, which result in the large jump in the energy curve of the FM  $Pnma$  phase in Figure 1.

When the compressive strain is larger than 1.5%, the FM  $Pnma$  structure

becomes unstable and the FM  $Cc$  structure is favored. This FM  $Cc$  phase is metallic, thus not FE. It should be noted that both  $Pnma$  and  $Cc$  phases were found in the simulations of epitaxial strained [-110]-oriented  $\text{BiFeO}_3$  thin film<sup>18</sup>. Interestingly, a phase transition from the FM metallic (FM- $M$ ) state to the A-AFM insulating FE (A-AFM- $I$ -FE) state occurs in the  $Cc$  structure at -6% strain. A similar phenomenon was also observed in a recent investigation on the epitaxial strained  $\text{SrCoO}_3$ <sup>17</sup>. This A-AFM- $Cc$  state with a band gap larger than 0.2 eV displays a large FE polarization and a relatively high  $T_N$  of ~304 K. As discussed in ref 17, in the vicinity of this phase transition, the magnetic-electric-elastic response may be expected due to the changes of the physical properties such as FE polarization, magnetic order, band gap and out-of-plane lattice parameter between the two phases. Thus we predict a possibility of a metal-insulator transition at a compressive strain in  $\text{BiMnO}_3$  thin films grown along the pseudocubic [001] direction. For examples, the A-AFM- $I$ -FE phase can be transformed into the FM- $M$  phase by applying magnetic field or a compressive uniaxial stress that will lead to an insulator-metal transition, while the opposite transition can be induced by applying electric field or a tensile uniaxial stress. Although these transitions occur at a large strain at 0 K in our study, the strain may be reduced at a finite temperature according to the reports on the other FE perovskite thin films (ref 19 and references therein).

In the tensile strain region, there is a phase transition at 2% strain from the PE-FM  $Pnma$  state to FE-FM  $Cc$  state. Although it is hard to tell whether the A-AFM  $Cc$  state has lower energy than the FM  $Cc$  state, the total energy and extracted

out-of-plane spin exchange parameters (see Part 1 of SI) provide unambiguous evidence that the FM order is preferred. In particular, the FM order is much more stable than the A-AFM order within the 2–3% strain region. The magnetic Curie temperature for the FM  $Cc$  state at 2% strain is estimated to be  $T_c \sim 395\text{K}$  within the mean field approximation. We find that the FM  $Cc$  state has an electric polarization as large as  $80 \mu\text{C}/\text{cm}^2$ . As expected from the polarization-strain coupling characteristic of the ferroelectric perovskites, the in-plane polarization ( $P_{xy}$ ) of FM- $Cc$  state increases with the increasing strain whereas the out-of-plane polarization ( $P_z$ ) decreases, while the opposite behaviors are found for A-AFM  $Cc$  state in the compressive region (see Figure 2a). Therefore, we predict that the tensile strain could stabilize a high temperature FM-FE phase in  $\text{BiMnO}_3$  thin film. Interestingly, the predicted low temperature FM-FE phase in  $\text{EuTiO}_3$  thin films was confirmed by a recent experiment<sup>2</sup>.

For all the new three phases (A-AFM-FE  $Cc$ , FM-PE  $Pnma$  and FM-FE  $Cc$  phases) of  $\text{BiMnO}_3$  predicted in this work, we find that each Mn ion has two long Mn-O bonds along the local  $z$  axis and four short Mn-O bonds in the local  $xy$ -plane. Thus, the  $\text{Mn}^{3+}$  ion ( $d^4$ ) has the  $t_{2g}^3 d_{z^2}^1$  electron configuration. Indeed, the partial charge distribution (Figures 3a-3c) shows that the highest occupied  $d$  state is  $d_{z^2}$ -like. Interestingly, we find that the orbital orders of Mn ions for the three phases are different from each other. In the A-AFM-FE  $Cc$  phase, the Mn ions have an occupied  $d_z^2$  orbital along the  $c$ -axis, while the occupied  $d_z^2$  orbitals of Mn ions lie in the  $ab$ -plane for the FM-PE  $Pnma$  phase where the  $d_z^2$  orbital is approximately orthogonal

to the in-plane nearest neighbors, but parallel to the out-of-plane nearest neighbors, similar to the  $\text{LaMnO}_3$  case. As for the FM-FE  $Cc$  phase, it has a similar in-plane arrangement of the  $d_z^2$  orbital as the FM-PE  $Pnma$  phase, but an almost orthogonal arrangement between the adjacent planes along the  $c$ -axis. The orbital orders lead to the magnetic ground states of the three phases, as shown in the third part of SI.

In order to study why the  $Cc$  structure can generate such a large FE polarization, we calculate the polarization by summing the product of the ions displacements with the Born effective charges in the  $Cc$  structure at 3% strain. The reference paraelectric structure ( $C2/c$  space group) is obtained by adding the centrosymmetric operation to the  $Cc$  structure. Then we find that the contributions of  $\text{Bi}^{3+}$ ,  $\text{Mn}^{3+}$ ,  $\text{O}^{2-}$  ions to the total polarization are (30.762, 28.043, 27.291), (0.684, -0.957, -0.061), (18.887, 23.227, 10.168)  $\mu\text{C}/\text{cm}^2$ , respectively. So, this large polarization is mainly due to the displacements of  $\text{Bi}^{3+}$ ,  $\text{O}^{2-}$  ions. To find out the origins of these displacements, we calculate the electron localization function for the state. As shown in Figure 3d, the  $6s^2$  lone pairs are distributed along the same directions, which is different from the situation of  $C2/c$  bulk structure in which the  $\text{Mn}^{3+}$  ions arranged along the  $b$ -axis have the opposite distributions of  $6s^2$  lone pairs viewed from the  $c$ -axis<sup>13</sup>. Therefore the  $\text{Bi}^{3+}$  ions move along the same directions. The final displacements of  $\text{Bi}^{3+}$ ,  $\text{O}^{2-}$  ions are found to be along the pseudocubic  $[11z]$  direction because of the existence of glide plane lying in the (1-10)-plane ( $bc$ -plane in Figure 3d), which result in the  $[11z]$  direction of the FE polarization. The ferroelectricity induced by the epitaxial strain in the  $Cc$  structure may be due to the long-range Coulomb interactions related to the Bi



ions, different from the strained  $\text{CaMnO}_3$  case where the  $\text{Mn}^{4+}$  ions are responsible for the ferroelectricity<sup>15</sup>.

So far, we have predicted the coexistence of the ferromagnetism and ferroelectricity in the  $Cc$  phase (strain > 2%). The FM-FE  $Cc$  structure is also found to be dynamically stable (see Figure S4 of SI). And the ground state nature of the FM-FE  $Cc$  structure is further confirmed by our global optimization genetic algorithm simulations<sup>30</sup>. Another important question is that whether there exists magnetoelectric coupling between the two ferroic orders in the phase. First, we calculate the single-ion anisotropy (SIA) of  $\text{Mn}^{3+}$  ion in the  $Cc$  structure at 3% strain using DFT+U+SOC method. The results show that the  $\text{Mn}^{3+}$  ion has an easy-axis anisotropy with the local easy-axis close to the longest Mn-O bond direction, as shown in Figure 3d. The direction of the easy axis can be explained by the second order perturbation theory, similar to the  $\text{TbMnO}_3$  case<sup>31</sup>. As a result, the easy magnetization axis of the FM state will be nearly in the  $ab$ -plane because all four local easy axes are almost in the plane. The total SIA energy of the FM  $Cc$  state can be written as  $E_{\text{SIA}} = \sum_i A(\mathbf{S}_i \cdot \mathbf{n}_i)^2$ , where  $A = -3.105$  meV/Mn is the effective single-ion anisotropic parameter,  $\mathbf{S}_i = \mathbf{S}(\theta, \varphi)$  represents the  $i$ -th  $\text{Mn}^{3+}$  spin direction ( $\theta$  and  $\varphi$  are the zenith and azimuth angles of the magnetization direction defined in the pseudocubic coordination system), and  $\mathbf{n}_i$  is the direction of the local easy-axis. We then find that the total SIA energy is the lowest when  $\theta = 90^\circ$  and  $\varphi = 135^\circ$ , i.e., the pseudocubic [1-10] direction (see part 5 of SI). We can see that the easy magnetization axis is orthogonal to the direction of the electric polarization. The hard magnetization axis is along the

direction with  $\theta \approx 165^\circ$  and  $\varphi = 45^\circ$ . The energy difference between the hard magnetization case and the easy magnetization case is as large as  $|A|/2 \approx 1.55$  meV/Mn. When the spins are in the *ab*-plane ( $\theta = 90^\circ$ ),  $E_{\text{SIA}}(\phi) \sim B \sin(2\phi)$  ( $B > 0$ ). The  $\sin(2\phi)$  dependence of the total energy is in good agreement with the results from the direct DFT+U+SOC calculations (Figure 4a square dots).

Because the low symmetry of the *Cc* structure, we would expect that there will exist eight different FE domains with different polarizations  $P = (\pm x_0, \pm x_0, \pm z_0)$ . The easy magnetization axis of the four FE domains [ $P = (x_0, x_0, z_0)$ ,  $P = (x_0, x_0, -z_0)$ ,  $P = (-x_0, -x_0, z_0)$ ,  $P = (-x_0, -x_0, -z_0)$ ] will be almost orthogonal to that of the other four domains [ $P = (x_0, -x_0, z_0)$ ,  $P = (x_0, -x_0, -z_0)$ ,  $P = (-x_0, x_0, z_0)$ ,  $P = (-x_0, x_0, -z_0)$ ]. From the above discussions, we propose that there should exist intrinsic magnetoelectric coupling in the FM-FE *Cc* phase: The two types of domains can be switched by the external electric field, thus the  $\text{Mn}^{3+}$  spins directions can be controlled by an electric field (see Figure 4b). The control of the magnetic order by the electric field was predicted in previous first principles calculations<sup>2,3,17</sup>, in which it occurs at the phase boundary between two phases with different magnetic and polar orders. Experimentally<sup>32,33</sup>, a ferroelectric control of spin direction was also demonstrated: The control of the spin direction arises from the pure interface effect where the switch of the FE polarization of the bottom ferroelectric layer induces the changes of the magnetic anisotropy of the top layer. However, the strong magnetoelectric coupling due to the strong SIA of Mn ion predicted in this FM-FE *Cc* phase is intrinsic. The

mechanism for manipulating magnetization vector by electric fields proposed in this work is also different from that in the diluted magnetic semiconductor case [e.g., (Ga,Mn)As], where an electric field tunes the hole concentration and thus the magnetic anisotropy<sup>34</sup>. Furthermore, the novel intrinsic magnetoelectric coupling revealed in this study does not require the same magnetic ion to be responsible for both ferroelectricity and magnetism, suggesting a new direction for searching new multiferroics.

## CONCLUSIONS

In summary, we performed first principles calculations to investigate the effects of the epitaxial strain on the properties of BiMnO<sub>3</sub> films grown along the pseudocubic [001] direction. Unlike the ground state of the centrosymmetric  $C2/c$  space group in bulk, three previously unreported phases, namely, A-AFM  $Cc$ , FM  $Pnma$  and FM  $Cc$  phases, are observed under epitaxial strain. For tensile strain larger than 2%, the  $Cc$  structure has a large electric polarization ( $P > 80 \mu\text{C}/\text{cm}^2$ ) and is FM with a high magnetic Curie temperature (estimated  $T_c \sim 395 \text{ K}$ ). To the best of our knowledge, BiMnO<sub>3</sub> under tensile strain has the highest Curie temperature among all FM-FE multiferroics. Moreover, a novel intrinsic magnetoelectric coupling is predicted to exist in the FM-FE  $Cc$  phase with the easy axis tunable by the external electric field, which indicates the potential application of epitaxial (001) BiMnO<sub>3</sub> thin films in spintronic devices.

## ACKNOWLEDGMENT

Work at Fudan was partially supported by NSFC, the Special Funds for Major State Basic Research, Foundation for the Author of National Excellent Doctoral Dissertation of China, The Program for Professor of Special Appointment at Shanghai Institutions of Higher Learning, Research Program of Shanghai municipality and MOE.

\*Electronic address: [hxiang@fudan.edu.cn](mailto:hxiang@fudan.edu.cn)

## REFERENCES

- (1) (a) Cheong, S.-W.; Mostovoy, M. *Nature Mater.* **2007**, 6, 13. (b) Ramesh, R.; Spaldin, N. A. *Nature Mater.* **2007**, 6, 21. (c) Picozzi, S.; Ederer, C. *J. Phys.: Condens. Matter* **2009**, 21, 303201. (d) Wang, K. F.; Liu, J.-M.; Ren, Z. F. *Adv. Phys.* **2009**, 58, 321. (e) Khomskii, D. *Physics* **2009**, 2, 20. (f) Xiang, H. J.; Kan, E. J.; Zhang, Y.; Whangbo, M.-H.; Gong, X. G. *Phys. Rev. Lett.* **2011**, 107, 157202.
- (2) (a) Fennie, C. J.; Rabe, K. M. *Phys. Rev. Lett.* **2006**, 97, 267602. (b) Lee, J. H. *et al. Nature* **2010**, 466, 954.
- (3) Lee, J. H.; Rabe, K. M. *Phys. Rev. Lett.* **2010**, 104, 207204.
- (4) Hill, N. A.; Rabe, K. M. *Phys. Rev. B* **1999**, 59, 8759.
- (5) Faqir, H. *et al. J. Solid State Chem.* **1999**, 142, 113.
- (6) Moreira dos Santos, A. *et al. Solid State Commun.* **2002**, 122, 49.
- (7) Moreira dos Santos, A. *et al. Phys. Rev. B* **2002**, 66, 064425.

- (8) Kimura, T. *et al. Phys. Rev. B* **2003**, 67, R180401.
- (9) Montanari, E. *et al. Chem. Mater.* **2005**, 17, 1765.
- (10) Belik, A.; Takayama-Muromachi, E. *Inorg. Chem.* **2006**, 45, 10224.
- (11) Belik, A. *et al. J. Am. Chem. Soc.* **2007**, 129, 971.
- (12) Montanari, E. *et al. Phys. Rev. B* **2007**, 75, R220101.
- (13) Baettig, P.; Seshadri, R.; Spaldin, N. A. *J. Am. Chem. Soc.* **2007**, 129, 9854.
- (14) Goian, V. *et al. J. Appl. Phys.* **2012**, 112, 074112.
- (15) Bhattacharjee, S.; Bousquet, E.; Ghosez, Ph. *Phys. Rev. Lett.* **2009**, 102, 117602.
- (16) Dupé B.; Prosandeev, S.; Geneste, G.; Dkhil, B.; Bellaiche, L. *Phys. Rev. Lett.* **2011**, 106, 237601.
- (17) Lee, J. H.; Rabe, K. M. *Phys. Rev. Lett.* **2011**, 107, 067601.
- (18) Prosandeev, S.; Kornev, I. A.; Bellaiche, L. *Phys. Rev. Lett.* **2011**, 107, 117602.
- (19) Yang, Y. R.; Ren, W.; Stengel, M.; Yan, X. H.; Bellaiche, L. *Phys. Rev. Lett.* **2012**, 109, 057602.
- (20) Liechtenstein, A. I.; Anisimov, V. I.; Zaanen, J. *Phys. Rev. B* **1995**, 52, R5467.
- (21) Perdew, J. P. *et al. Phys. Rev. Lett.* **2008**, 100, 136406.
- (22) (a) Blöchl, P. E. *Phys. Rev. B* **1994**, 50, 17953. (b) Kresse, G.; Joubert, D. *Phys. Rev. B* **1999**, 59, 1758.
- (23) Kresse, G.; Furthmüller, J. *Comput. Mater. Sci.* **1996**, 6, 15. *Phys. Rev. B* **1996**, 54, 11169.
- (24) (a) King-Smith, R. D.; Vanderbilt, D. *Phys. Rev. B* **1993**, 47, 1651. (b) Resta, R. *Rev. Mod. Phys.* **1994**, 66, 899.

- (25) Zayak, A. T.; Huang, X.; Neaton, J. B.; Rabe, K. M. *Phys. Rev. B* **2006**, *74*, 094104.
- (26) Hatt, A. J.; Spaldin, N. A. *Phys. Rev. B* **2010**, *82*, 195402.
- (27) Rushchanskii, K. Z.; Spaldin, N. A.; Lezaic, M. *Phys. Rev. B* **2012**, *85*, 104109.
- (28) Stokes, H. T.; Kisi, E. H.; Hatch, D. M.; Howard, C. J. *Acta Crystallogr. Sect. B* **2002**, *58*, 934.
- (29) Hatt, A. J.; Spaldin, N. A. *Eur. Phys. J. B* **2009**, *71*, 435.
- (30) (a) Xiang, H. J.; Wei, S.-H.; Gong, X. G. *Phys. Rev. B* **2010**, *82*, 035416. (b) Xiang *et al.* unpublished.
- (31) Xiang, H. J.; Wei, Su-Huai; Whangbo, M.-H.; Juarez L. F. Da Silva *Phys. Rev. Lett.* **2008**, *101*, 037209.
- (32) Garcia, V. *et al. Science* **2010**, *327*, 1106.
- (33) Mardana, A.; Ducharme, S.; Adenwalla, S. *Nano Lett.* **2011**, *11*, 3862.
- (34) Chiba, D.; Sawicki, M.; Nishitani, Y.; Nakatani, Y.; Matsukura, F.; Ohno, H. *Nature* **2008**, *455*, 515.

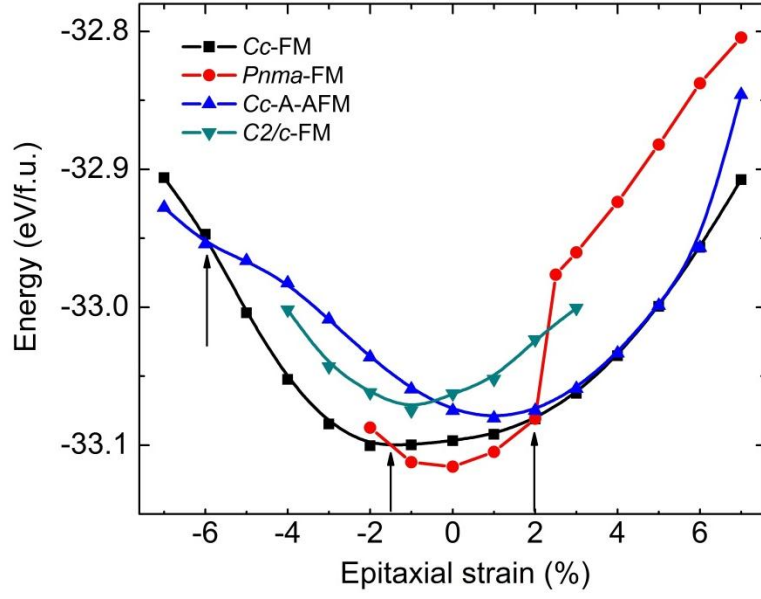


Figure 1. Calculated total energies versus the epitaxial strains for the various spin orders with  $Pnma$  and  $Cc$  space groups. The total energies of the FM  $C2/c$  phase are also plotted over the range from -4% to +3% for comparison. The vertical black lines at -6%, -1.5% and 2% indicate the phase boundaries between A-AFM- $I$ -FE  $Cc$ , FM- $M$   $Cc$ , FM- $I$ -PE  $Pnma$ , and FM- $I$ -FE  $Cc$  phases, respectively.

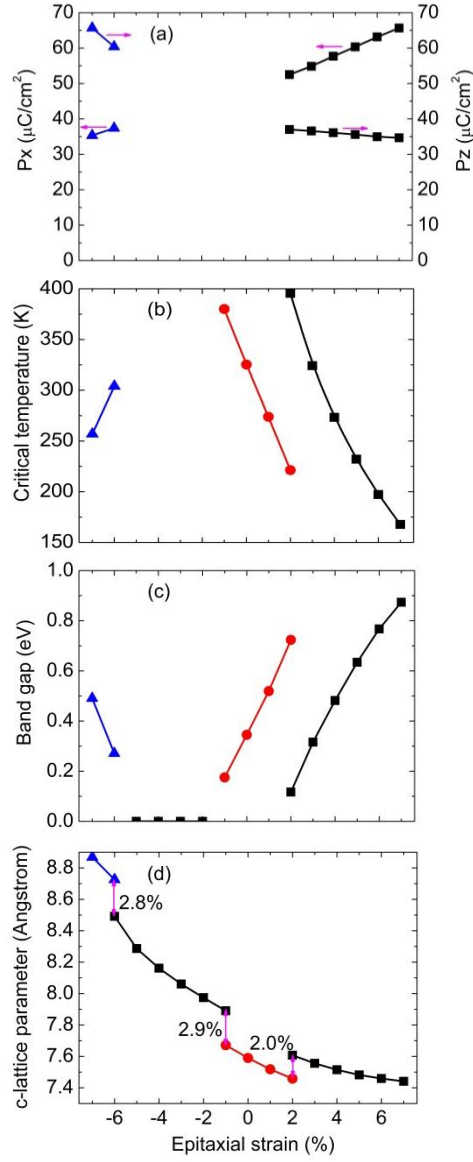


Figure 2. Physical properties of epitaxial (001) BiMnO<sub>3</sub> thin film in the lowest energy state at each strain. (a) Calculated ferroelectric polarization ( $P_y = P_x$ ). (b) Magnetic critical temperatures of FM and A-AFM orders. (c) Band gap. (d) *c*-lattice parameter. Symbols are the same as those in Figure 1.



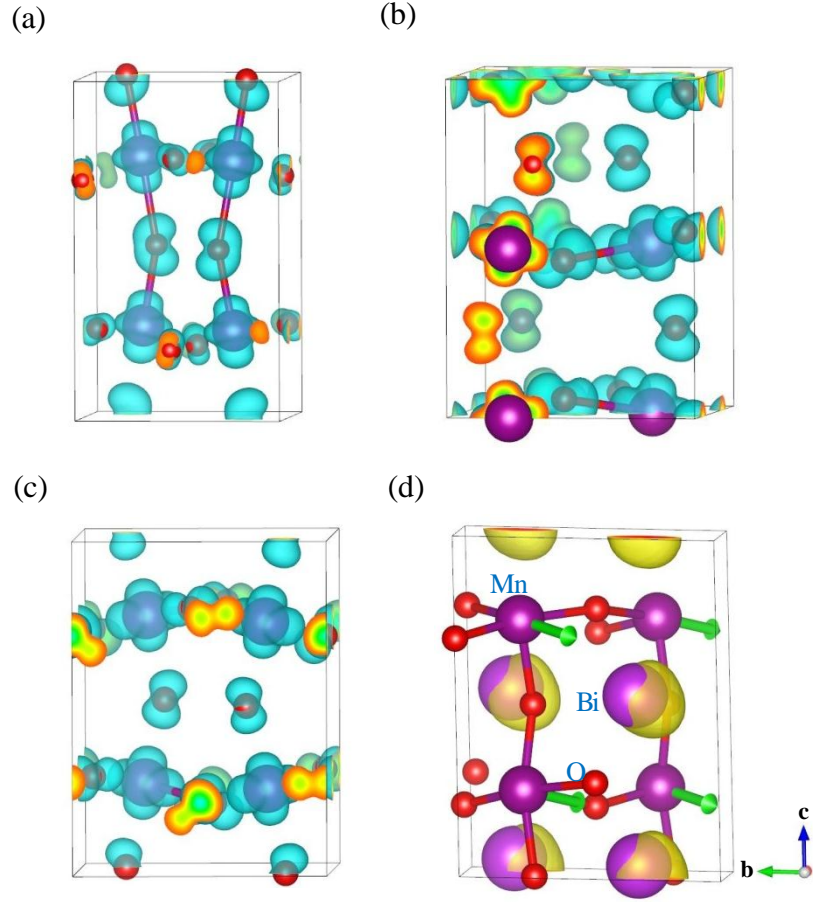


Figure 3. Orbital orders in (a) A-AFM  $Cc$  structure at -6% strain, (b) FM  $Pnma$  structure at 0 % strain and (c) FM  $Cc$  structure at 3% strain. Only long Mn-O bonds are shown and Bi ion has been removed for clarity. (d) Isosurface of the electron localization function with the value of 0.8 for the FM  $Cc$  structure at 3% strain. The green arrow indicates the easy-axis of the  $Mn^{3+}$  ion.

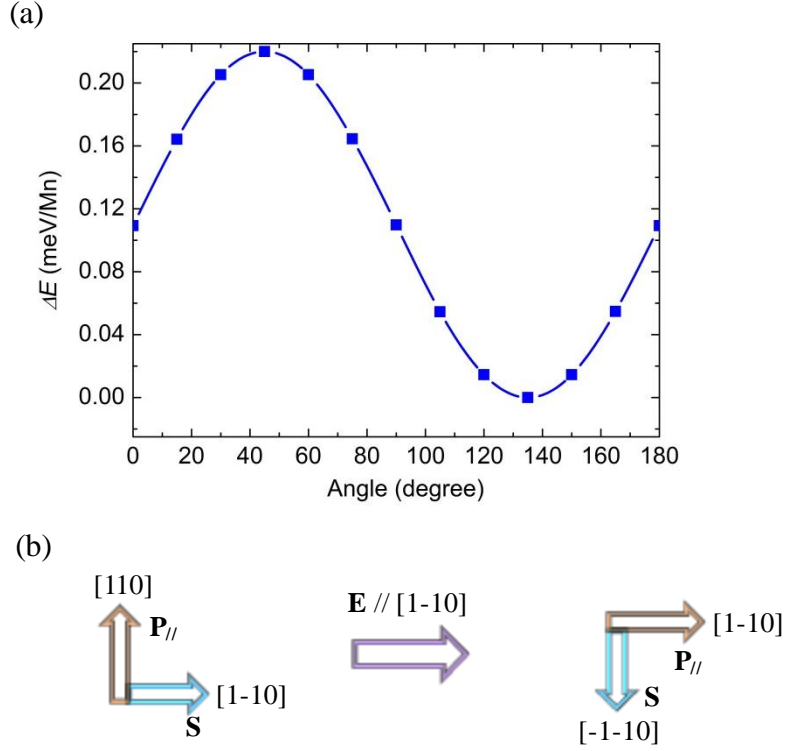


Figure 4. (a) Total energy (Square dots) of the FM  $Cc$  structure at 3% strain from the DFT+U+SOC calculations as a function of the angle between the magnetization direction and the pseudocubic [100]-direction when the magnetization is rotated in the  $ab$ -plane. The line is the fitted result using the single-ion anisotropy model defined in the text. (b) Schematic illustration of the magnetoelectric coupling in the FM-FE  $Cc$  phase.  $\mathbf{P}$ ,  $\mathbf{S}$  and  $\mathbf{E}$  represent the FE polarization, Mn spin and external electric field, respectively. Here the directions are defined within the pseudocubic setting.

**High Temperature Ferromagnetic-Ferroelectric Multiferroicity in  
Strained BiMnO<sub>3</sub>**

***Supporting Information***

X. Z. Lu, X. G. Gong, and H. J. Xiang<sup>\*</sup>

Key Laboratory of Computational Physical Sciences (Ministry of Education), State

Key Laboratory of Surface Physics, and Department of Physics, Fudan University,

Shanghai 200433, P. R. China

<sup>\*</sup>e-mail: [hxiang@fudan.edu.cn](mailto:hxiang@fudan.edu.cn)

## 1. Values for the spin exchange parameters

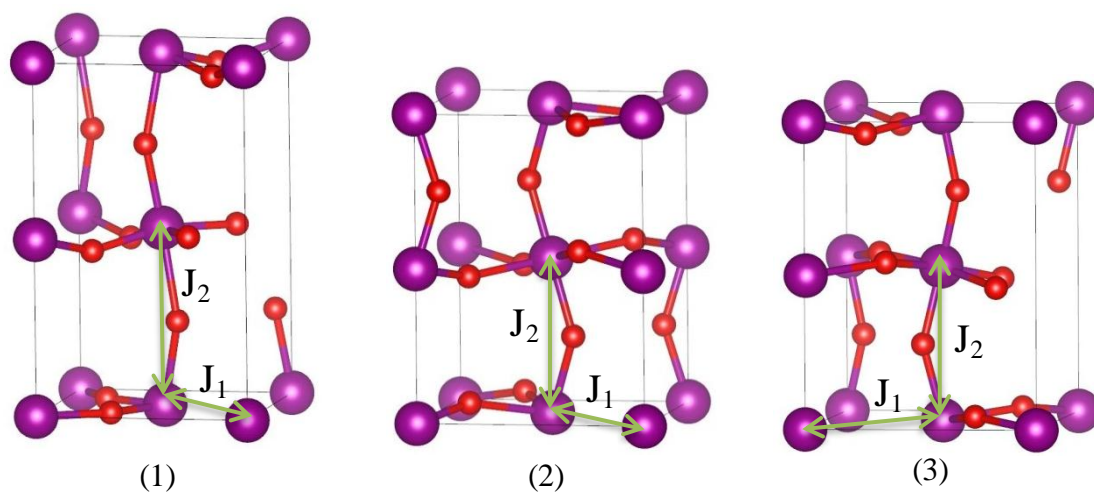


Figure S1. Representative structures. (1) A-AFM-FE  $Cc$  structure at -6% strain, (2) FM-PE  $Pnma$  structure at 0 % strain and (3) FM-FE  $Cc$  structure at 3% strain. The spin exchange paths  $J_1$ - $J_2$  in the selected structures are also shown. Bi ion has been removed for clarity.

Table S1. Calculated exchange parameters (J) deduced from GGA+U calculations, where  $J_i$  is an effective spin exchange value obtained by setting  $|\mathbf{S}_i| = 1$ , namely,  $J_{ij}^{\text{eff}} = J_{ij}\mathbf{S}_i\mathbf{S}_j$  for a spin dimer  $ij$ .

Strain (%)	$J_1$ (meV)	$J_2$ (meV)
-7	-3.293	15.550
-6	-7.122	11.949
-1	-13.086	-6.583
0	-11.335	-5.359
1	-9.628	-4.339
2 <sup>*</sup>	-7.634	-3.799
2 <sup>**</sup>	-15.458	-3.158
3	-12.964	-2.006
4	-11.138	-1.277
5	-9.596	-0.808
6	-8.290	-0.417
7	-7.170	-0.113

Note: The superscript \* represents the value for the FM *Pnma* structure and \*\* for the FM *Cc* structure.

## 2. Energy difference between $C2/c$ and $C2$ structures

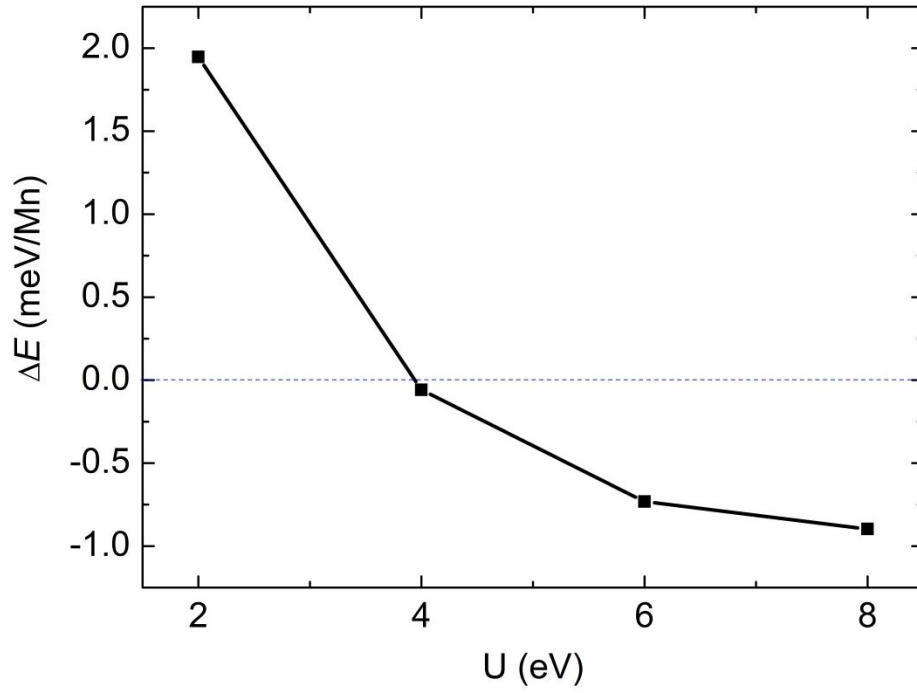
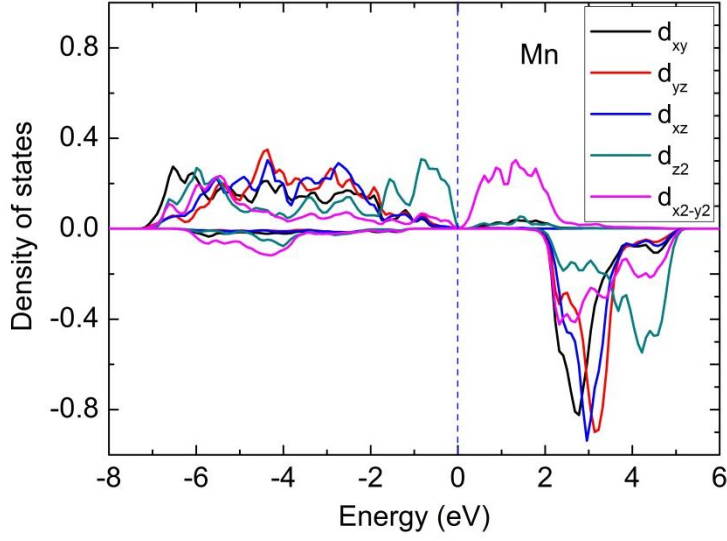


Figure S2. Energy difference between  $C2/c$  and  $C2$  structures with the FM spin order versus the on-site repulsion  $U$ . When  $U$  is larger than 4 eV, the  $C2/c$  structure becomes more stable, in agreement with the experimental result<sup>1</sup>. Therefore,  $U = 4$  eV is adopted in our calculations.

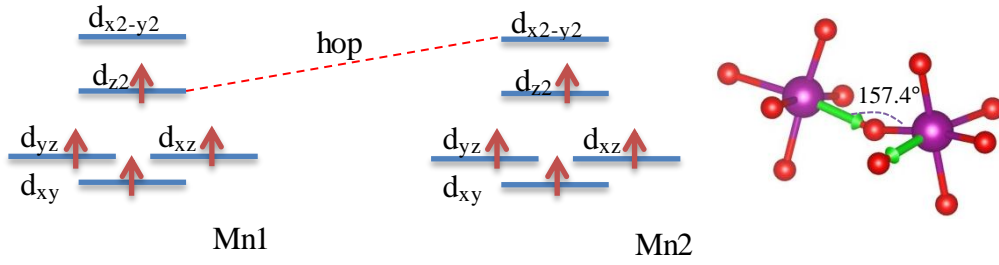
### 3. Origin of the magnetic ground state

(a)



(b)

In-plane case



Out-of-plane case

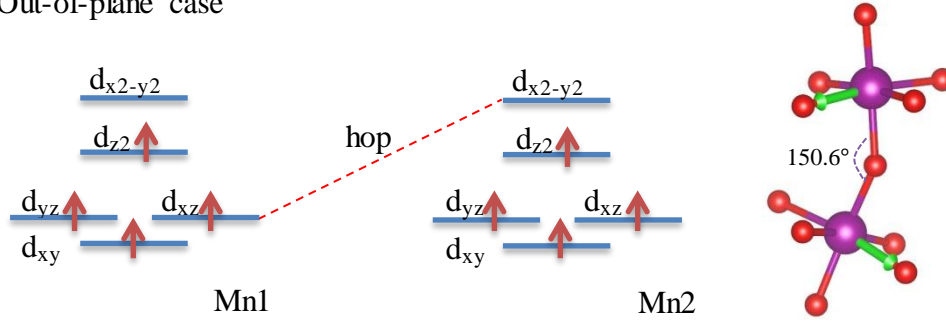


Figure S3. (a) Partial density of states for the  $Cc$  structure at 3% strain with a 0.1 eV broadening. The d orbitals refer to the local coordination system, where the z axis is along the long Mn-O bond direction. (b) Left panel: Schematic illustration of  $\sigma - \sigma$  coupling and  $\sigma - \pi$  coupling for the in-plane and out-of-plane cases, respectively. Right panel: Corresponding Mn1-O-Mn2 angles in the two cases. Green arrow

indicates the local  $z$  axis.

The results depicted in Figure S3 show that the coupling between the nearest neighbors of Mn ions in the in-plane is a strong  $\sigma - \sigma$  coupling between the occupied  $d_{z^2}$  orbital in Mn1 and the unoccupied  $d_{x^2-y^2}$  orbital in Mn2, while a  $\sigma - \pi$  coupling takes place between the occupied  $d_{yz}/d_{xz}$  orbitals in Mn1 and unoccupied  $d_{x^2-y^2}$  orbital in Mn2 for the out-of-plane nearest-neighbors because of the small energy difference between them. Thus the magnetic order for the FM-FE  $Cc$  phase is ferromagnetic. The similar explanations are also expected for the A-AFM-FE  $Cc$  and FM-PE  $Pnma$  phases.



#### 4. Phonon spectrum for the *Cc* structure at 3% strain

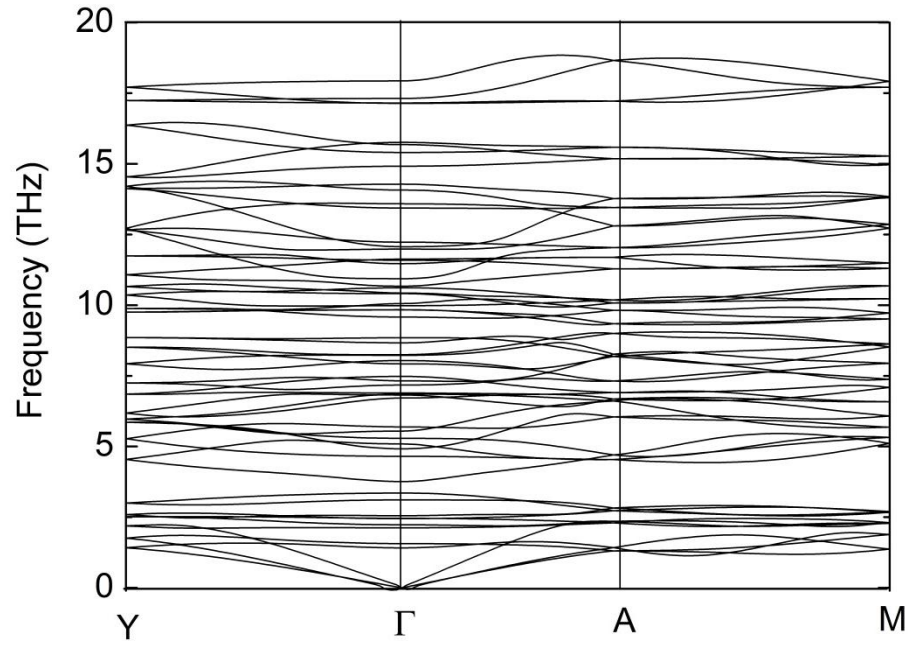


Figure S4. Phonon spectrum for the *Cc* structure at 3% strain. The phonon frequencies are calculated using the frozen phonon method in  $2 \times 2 \times 2$  supercell with a  $2 \times 2 \times 1$   $k$ -point mesh at the  $\Gamma$ , A, M and Y points of Brillouin zone of 20-atom cell. The figure indicates that the structure is dynamically stable.

## 5. The total single-ion anisotropic energy of the FM $Cc$ state at 3% strain

We compute the total single-ion anisotropic energy of the FM  $Cc$  state by using the following equation:

$$\begin{aligned}
 E_{\text{SIA}} &= \sum_i A(\mathbf{S}_i \cdot \mathbf{n}_i)^2 \\
 &= 2A(\sin^2 \theta (n_{1x}^2 + n_{1y}^2) + 2 \cos^2 \theta n_{1z}^2 + 4 \sin^2 \theta \sin \varphi \cos \varphi n_{1x} n_{1y} \\
 &\quad + 2 \sin \theta \cos \theta (\sin \varphi + \cos \varphi)(n_{1x} + n_{1y})n_{1z})
 \end{aligned} \tag{1}$$

where  $E_{\text{SIA}}$  is the total single-ion anisotropic energy,  $A = -3.105$  meV/Mn is the effective single-ion anisotropic parameter,  $\mathbf{S}_i = \mathbf{S}(\theta, \varphi)$  represents the  $i$ -th  $\text{Mn}^{3+}$  spin ( $|\mathbf{S}_i| = 1$ ) where  $\theta$  and  $\varphi$  of the sphere coordinates determine the spin direction, and  $\mathbf{n}_i$  the direction of its easy-axis where  $n_{1x} = 0.036$ ,  $n_{1y} = -0.984$  and  $n_{1z} = -0.176$  are the Cartesian components of  $\mathbf{n}_i$ . To find the extreme value of  $E_{\text{SIA}}$ , we need to solve the following equations:

$$\begin{cases} \tan 2\theta = -\frac{2n_{1z}(n_{1x} + n_{1y})(\sin \varphi + \cos \varphi)}{n_{1x}^2 + n_{1y}^2 - 2n_{1z}^2 + 4 \sin \varphi \cos \varphi n_{1x} n_{1y}} \end{cases} \tag{2}$$

$$\begin{cases} \cos^2 \varphi - \sin^2 \varphi = -\frac{\cos \theta n_{1z}(n_{1x} + n_{1y})(\cos \varphi - \sin \varphi)}{2 \sin \theta n_{1x} n_{1y}} \end{cases} \tag{3}$$

Situation (i):  $\cos \varphi = \sin \varphi$ , i.e.,  $\varphi = 45^\circ$ , then  $\theta \approx 165^\circ$  can be obtained by Eq.

(2). In this case,  $E_{\text{SIA}} = 0$  is the maximum value.

Situation (ii):  $\cos \varphi \neq \sin \varphi$ , then Eq. (3) becomes

$$\sin \varphi + \cos \varphi = -\frac{\cos \theta n_{1z}(n_{1x} + n_{1y})}{2 \sin \theta n_{1x} n_{1y}} \tag{3'}$$

Since Eq. (2) and Eq. (3) are self-consistent, then the solutions are  $\theta = 90^\circ$  and  $\varphi = 135^\circ$ . The result shows that  $E_{\text{SIA}} \approx 2A$  is the minimum value. Therefore, the FM  $Cc$  state has a strong anisotropy with an energy difference of 1.55 meV/Mn

between the hard magnetization case and the easy magnetization case.

**Reference:**

(1) Montanari, E. *et al. Phys. Rev. B* **2007**, 75, R220101.